Development of Ice Load Maps for Structural Design

Bjørn Egil Nygaard[1], Kristian Ingvaldsen[1], Øyvind Welgaard[2]

[1] *Kjeller Vindteknikk (part of Norconsult), Norway*
[2] *Statnett SF, Norway*

Bjorn.Egil.Nygaard@vindteknikk.com, Kristian.Ingvaldsen@norconsult.com, Øyvind.Welgaard@statnett.no

Abstract— **This paper presents the various stages in the development of a high-resolution ice load map of Norway. The map is intended for planning and design of the electrical power grid system in Norway. However, with some changes and additions, the map will also be applicable for design of other structures such as towers, masts, chimneys, ropeways, ski-lifts etc.**

The ice loads are modelled based on a hindcast dataset produced through dynamic downscaling of the global ECMWF ERA-5 reanalysis dataset. The downscaling simulations are carried out using Weather Research and Forecasting (WRF) model, running 31 years at 3 km x 3 km grid spacing, as well as two winters at 0,75 km x 0,75 km grid spacing. Statistical downscaling is applied to combine the two hindcast datasets before ice loads are calculated using appropriate time dependent ice accretion models. Finally, characteristic ice loads are estimated through tailored extreme value analysis methods. The hindcast data as well as the calculated ice loads are validated with field measurements from selected test sites and operational 420 kV transmission lines. In this paper we present the methodology, validation as well as some preliminary results.

Keywords— **characteristic ice load, mapping, hindcast data, icing model, validation**

I. INTRODUCTION

Actions on structures due to ice loading is an important component of structural design in cold climate. Characteristic ice loads, i.e., the extreme ice load with 50-years return period, is required input in the design phase, however, site-specific climatic data for proper ice load assessment is often limited.

Some countries provide basic guidelines on how to take ice loads into account in the design in national annexes to international standards, e.g., by providing tabulated values of characteristic ice loads per region or altitude, or general guidance or requirements for determination of local values taking topographic features into account. Particularly in countries or regions of complex terrain, the estimated ice loading can be associated with a large uncertainty, and underestimation can cause structural damage [1] [2] [3].

The spatial variation of ice loads, particularly in complex terrain, makes local ice load assessment challenging. Even when near-by icing measurements are available, the spatial representativity of the measurement data can be questioned due to local terrain induced variations in the both the wind field as well as in the cloud and precipitation variables. The great local variability is exemplified in [4] where two test spans located less than 1 km apart and with 70 m height difference show measured ice loads with nearly an order of magnitude in difference.

While the existing power grid in Norway has been designed according to ice loads derived from measurements and/or qualitative assessments performed by specialized meteorologists, numerical atmospheric models have now become an invaluable tool for assessment of local icing climate [5] - [6].

In the present study, a state-of-the-art numerical atmospheric model is used together with ice accretion models to generate a detailed icing climatology for Norway. The icing simulations are validated against available ice load measurements, and subsequently subjected to extreme value analyses to generate high-resolution maps of 50-year ice loads. The nation-wide ice load maps are currently being processed, so in this paper we show preliminary results for a smaller region. The work is carried out as a part of the Icebox research project [7], led by the Norwegian transmission system operator, Statnett.

II. METHODOLOGY

The various stages in the development of the icing map are described individually in sections A. – D. Finally, in section E, the complete structure of the data processing and analyses are summarized and visualized in a flow-chart.

A. *Hindcast data*

The atmospheric hindcast data is prepared with the Weather Research and Forecasting (WRF) model version WRF-ARW 4.1.2. It is a state-of-the-art mesoscale atmospheric model, used both for operational forecasting and for hindcasting [8].

A long-term hindcast simulation is produced by simulating the period 1990 – 2021 for a domain covering Norway, Sweden, Finland and Denmark at 3 km horizontal grid spacing (Fig. 1), corresponding to 401 856 grid points horizontally.

The high-resolution hindcast is produced with the same model setup, but at a horizontal grid spacing of 0,75 km for the three sub-domains shown in Fig. 2. The simulation covers two years (winter season only), which were selected based on a set of criteria, such as storm frequency, distribution of wind speed and direction, measured ice loads etc.

All simulations are initiated and forced on the lateral boundaries by the ECMWF–ERA5 dataset [9]. The Thompson-Eidhammer aerosol aware microphysics scheme [10] is used for parameterization of the cloud and precipitation processes but with modifications to the melting layer

parameterization according to [11]. Parameterization schemes used are listed in Table 1.

TABLE 1 PARAMETERIZATION SCHEMES USED IN THE WRF SIMULATIONS

Type of scheme	Name and reference
Microphysics	Thompson-Eidhammer aerosol-aware [10]
Boundary layer	MYNN2 [12]
Radiation	RRTMG [13]
Land surface	Noah [14]

Fig. 1 WRF domain for the long-term hindcast simulation at 3 km horizontal grid spacing.

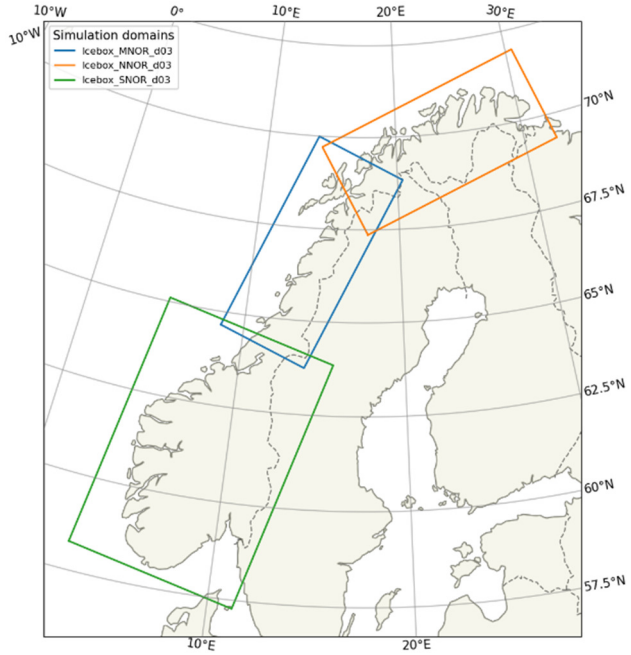

Fig. 2 WRF domains for the high-resolution hindcast simulation at 0,75 km horizontal grid spacing.

B. *Statistical downscaling*

Good predictions of ice accretion require detailed meteorological input data representing the local weather conditions as accurately as possible. Applications such as extreme value analysis and icing maps also impose requirements to the length and areal coverage of the input data set. However, producing a single dataset with sufficient resolution (i.e., 0,75 km grid spacing), length > 25 years and geographical extension covering all of Norway is both computationally and economically costly, and would extend far beyond the scope of this project.

The solution is therefore to combine the two data sets described in Section A. By doing so, one can obtain synthetic time series of key meteorological variables, such as liquid water content (LWC) and wind, that cover the entire time period of the coarse resolution data set while inheriting some of the qualities of the finer resolution, short-term data set. This can be done by applying different statistically downscaling methods. High-resolution representations of LWC and wind are particularly crucial because 1) both parameters are key predictors with regards to icing rates and 2) both parameters are greatly impacted by local topography through sheltering, orographic lifting and speed-up effects. In the present study, the LWC of the long-term dataset was downscaled using a multiple linear regression model developed through the Icebox project (described below), while the wind fields were downscaled using the methodology described as "Undheim-Nyhammer" in [15]. The wind correction method consists of a sector-wise quantile regression model that statistically links the high resolution and the coarse resolution datasets. for the overlapping time-period. When applied sector-wise, the sheltering and speed-up effects resolved in the high-resolution model are then statistically transferred to the long-term, coarse resolution dataset. The method is limited by the ability of the high-resolution model in resolving local terrain induced wind patterns, as well as by the length of the overlapping time-period.

Assuming that a relatively high-resolution model predicts LWC more accurately than a relatively low-resolution model, the LWC in the low-resolution model can be improved by adding the relative difference between the two models. Our analyses have shown that the difference in cloud water mixing ratio between two datasets of different horizontal resolution, ΔQc, can be estimated for each time step, t, using a multiple linear regression model with each of the hydrometeors in the low-resolution model as explanatory variables:

$$\Delta Qc(t, wd) \approx \beta_0(wd) + \beta_1(wd)Qc(t) + \beta_2(wd)Qr(t) + \beta_3(wd)Qs(t) + \beta_4(wd)Qg(t),$$

where Qc is the cloud water mixing ratio, Qr is the rain water mixing ratio, Qs is the snow mixing ratio, Qg is the graupel mixing ratio, β_0 is the y-intercept and β_1 – β_4 are the slope coefficients for each explanatory variable. The mixing ratios of snow, graupel and rain are all included in the regression model because precipitation particles tend to reduce the cloud water content through collision with and collection of cloud droplets. Cloud water mixing ratio corrections were made separately for eight different sectors to

account for wind direction dependencies, yielding β_n parameters as functions of wind direction (wd). The downscaled cloud water mixing ratio is then given as

$$Qc = Qc_{WRF3km} + \Delta Qc$$

As exemplified in Fig. 3, the impacts of LWC and wind corrections on the calculated ice loads are often significant. The figure compares measured ice loads on a high-altitude test span to simulated ice loads based on a low-resolution WRF model, a high-resolution WRF model as well as on the low-resolution model where the LWC and wind fields have been statistically downscaled using the high-resolution model.

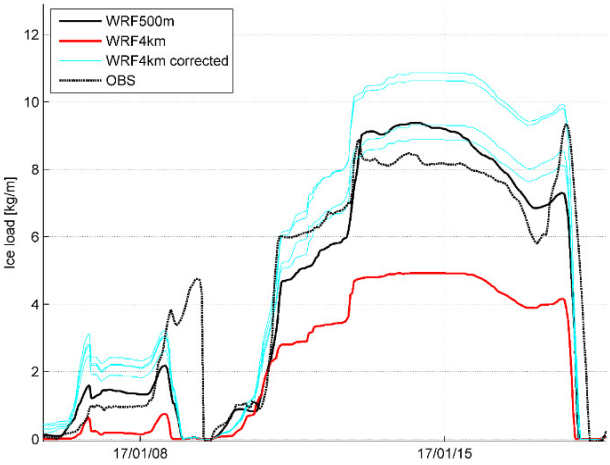

Fig. 3 Comparison of measured ice load (OBS) and simulated ice loads based on a low-resolution WRF model (WRF4km), a high-resolution WRF model (WRF500m) as well as on the WRF4km model where LWC and wind have been statistically downscaled using WRF500m. The four different "WRF4km corrected" lines are downscaled using four separate years from WRF500m.

C. *Ice accretion models*

1) *Model for rime ice:* Rime ice accretion is calculated based on the time dependent ice accretion model described in [16] and [17] with the methodology in [18] as discussed in [19]. The model includes rime icing (in-cloud) as well as freezing drizzle and freezing rain. The ice load is based on a temporal integration of the hourly icing rate which is calculated based on the simulated atmospheric data described above, which includes information on wind speed and supercooled atmospheric liquid water content. A detailed comparison between modelled and measured icing intensities at relevant test sites showed that among the different droplet size distribution discussed in [18] the best match was obtained here by assuming the "Langmuir J" distribution. A general underestimation of icing rates was found when testing the other, and more narrow Langmuir distributions.

2) *Model for wet snow:* The wet snow accretion model used in this study is similar to the one presented in [20]. However, a recalibration of the model is currently being carried out by comparison with a large dataset of observed wet snow loads in Iceland [21], with supplementary case studies from Norway and Sweden. The main findings can be summarized as follows:

- The cloud liquid water content should be included in the estimation of the liquid fraction of the snowflakes to avoid overestimated icing rates at exposed sites
- A reduction factor is introduced for the sticking efficiency, depending on the amount of graupel during wet snow events
- Allowance for dry snow accretion on already existing wet snow at low wind speed
- Precipitation intensity limit for the initiation of wet snow icing, calculated from the energy balance at the cylinder surface.

As discussed in [6], wet snow events are rare in nature, and their occurrences are sensitive to the ambient conditions. Even with more than 30 years of data there are relatively few events to base the extreme value analysis upon. In order to expand the basis for an extreme value analysis and obtain more robust estimates of return values, a post processing ensemble has been constructed. The ensemble consists of 40 different model runs, where the temperature is perturbed within the interval of ± 2 °C from the original model temperature. This is done for each single grid point in the entire model domain.

D. *Extreme value analysis*

Extreme values of rime icing are estimated by fitting a generalised extreme value distribution (GEV) to the annual maximum rime ice loads. This is done for each grid point individually, using the scikit-extremes package in python. 50-year ice loads are derived from the fitted distribution, and the procedure is repeated for each of the model time series representing the different line orientations.

Due to the rarity of wet snow events, annual maxima may not be the optimal selection of bulk maxima for extreme value analysis. The peaks-over-threshold (POT) extreme value analysis better suited for wet snow as all icing events are treated individually, and several events from the same year can be included in the analysis. The 50-year return values for wet snow are found through the following steps:

- Identify all icing events with the corresponding maximum value (peaks) from each of the 40 ensemble members
- Combine peaks from all ensemble members to one joint distribution (pooling)
- Define the threshold for the POT analysis
- Fit a generalised pareto distribution to the values exceeding the threshold.
- Derive a 50-year return value from the fitted distribution.

E. *Data processing overview*

The various stages in the development of ice load maps are summarized in Fig. 4 starting with the two hindcast simulations at the top, ending with the high- resolution ice load maps as results.

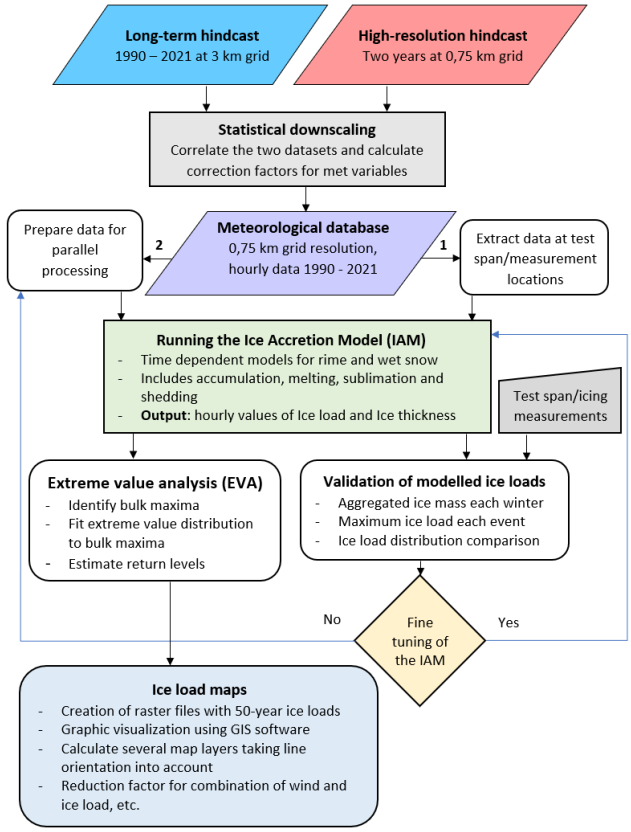

Fig. 4 Flow chart indicating the various stages in the development of ice load maps

III. RESULTS

A. Validation

The modelled ice loads are validated against available icing measurements, both from test spans, as well as from load cell measurements in operational 420 kV transmission lines. Table 2 presents an overview of the measurement data that was used in the validation study. All sites are located at relatively high altitude and are generally most exposed to rime icing. Extended data series of measured wet snow loads are non-existent in Norway, however, the model has been validated against an extensive dataset of observed wet snow loads in Iceland using a WRF hindcast dataset with identical set-up to the one described in section A. Although the model overestimated the observed wet snow loads in some areas, the results suggested that the model performed well in most parts of the country. Furthermore, the model has been validated against a set of individual wet snow observations in both Sweden and Norway (not shown in this paper).

TABLE 2 MEASUREMENT DATA OVERVIEW

Site	Elevation [m ASL]	Period	Type
Ålvikfjellet S	1086	2016.07.01 – 2021.07.01	Test span
Ålvikfjellet W	1088	2020.11.01 – 2022.01.21	Test span
Ålvikfjellet N	1015	2020.11.01 – 2022.01.21	Test span
Finseskaret	1420	2020.09.29 – 2022.01.21	420 kV line
Botnafjellet	1094	2020.09.29 – 2022.01.21	420 kV line
Litla Bjerangstinden	895	2020.09.29 – 2022.01.21	420 kV line

Being able to reproduce the measured distribution of ice load maxima with sufficient skill is key to obtain reliable extreme value estimates. Fig. 5 compares the measured and simulated distributions of rime ice load maxima at Ålvikfjellet during the period of available measurements (six years). The two data series were sorted individually, and only the 54 largest events from each series are shown. The distributions are quite similar, indicating that basis for extreme value analysis is reasonable. The full time series of measured and modelled rime ice loads at Ålvikfjellet are shown in .

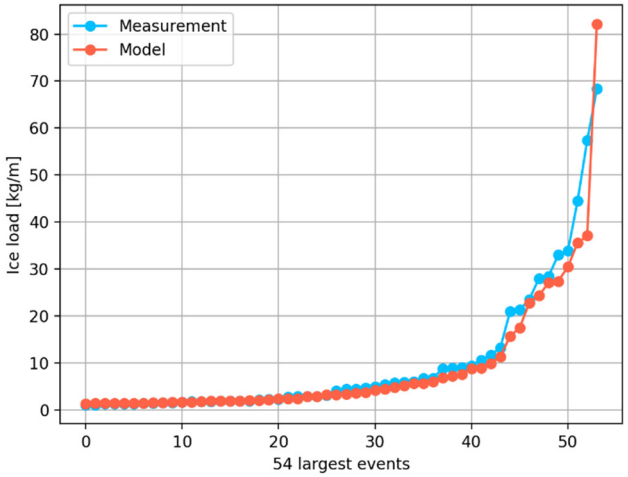

Fig. 5 Comparison of measured and modelled ice load maxima at Ålvikfjellet S ,1086 m asl. (red and blue lines, respectively). Ålvikfjellet is located just north of Hardangerfjorden in western Norway.

Even though most results suggest that the model performance is good, there are certain areas where the complexity of the local topography causes the model to struggle. Fig. 7 shows a comparison of measured and modelled ice load maxima at Finseskaret, located in a narrow ghat approximately 60 km east of Ålvikfjellet that is not resolved in the model terrain (not even at 750 m resolution). The results indicate that the model overestimates the measured ice load maxima, likely due to a lack of sheltering and/or channelling of the wind flow parallel to the power line. It should be noted, however, that the length of the dataset is considerably shorter compared to Ålvikfjellet (less than four months).

It should also be noted that despite being located 344 m higher than Ålvikfjellet, the ice loads are much smaller at Finseskaret, a difference which to a large extent is reproduced by the model.

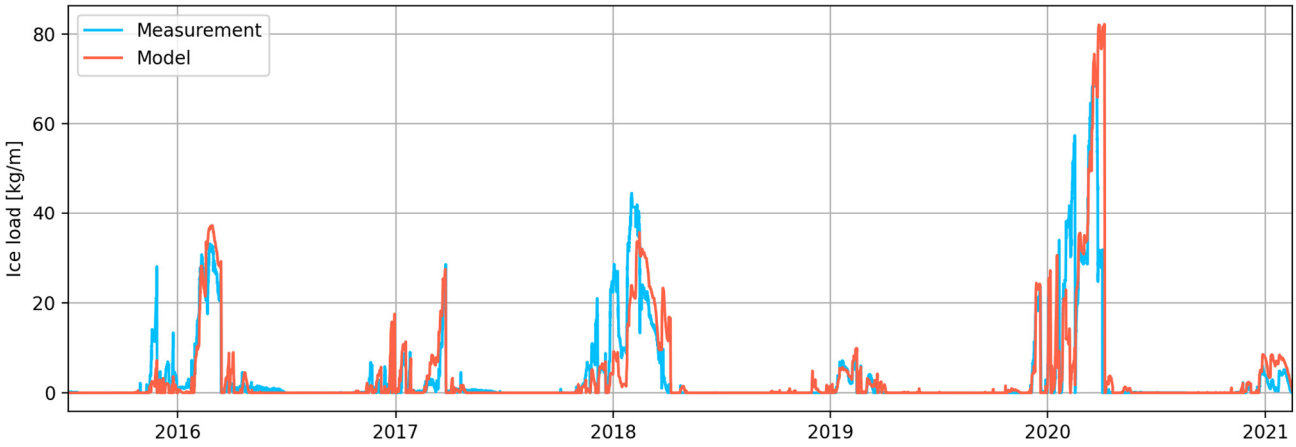

Fig. 6 Comparison of measured and modelled rime ice loads at Ålvikfjellet (read and blue lines, respectively).

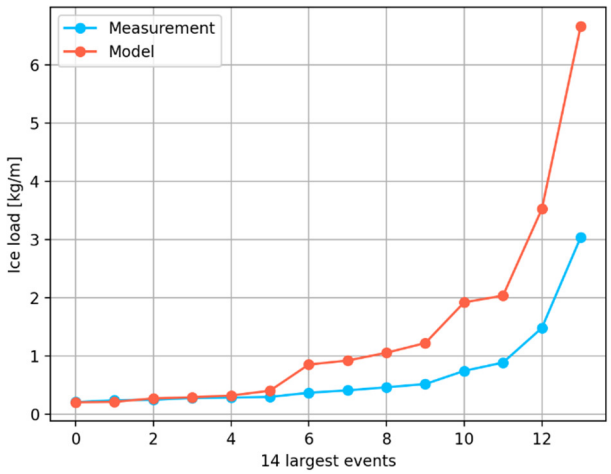

Fig. 7 Comparison of measured and modelled ice load maxima at Finseskaret, 1420 m asl. (red and blue lines, respectively).

B. Preliminary icing maps

Processing all the hindcast data through the statistical downscaling, ice accretion models as well as the extreme value analyses is computationally demanding, and even when utilizing high performance computing facilities, the complete analysis covering all of Noway takes several weeks[1]. In this paper a preliminary map for a limited area is shown in Fig. 8 as an example. The map was generated according to the methodology presented in Chapter II following the procedure summarized in Fig. 4, however, in this example the high-resolution dataset has a horizontal grid resolution of 0,5 km. For each single grid point, a GEV distribution was fitted to the annual maximum rime ice loads calculated on a reference collector.

In general, the map seems to reproduce many of the important characteristics of the rime ice climatology in this region:

- Rime icing is nearly non-existent in the low laying areas along the fjord and in the valleys.
- The ice loads increase rapidly with terrain height, particularly at sites exposed to moist air from south-west.
- Maximum values of several hundred kg/m are found at the most exposed mountain tops (not visible due to the limited color scale).
- Lower ice loads in sheltered areas compared to exposed areas at similar terrain height. E.g. the north-western corner compared to the hills along the Hardanger fjord.

Since the ice loads shown in the map are modelled assuming a reference object, the map could be used directly to specify characteristic ice loads for design of structures according to the ISO 12494 standard [16]. Furthermore, local height factors for rime ice can be assessed by utilizing multiple vertical levels from the hindcast data.

For overhead power lines the ice loads calculated on a reference object may be conservative due to the reduced icing on horizontal elements with a component parallel to the wind. Similar ice load maps were therefore calculated for different theoretical orientations of power lines. By implementing these map layers in a GIS tool, the ice load relevant for a given power line span, taking its orientation into account can be obtained directly.

[1] Estimated to be finalized during June 2022

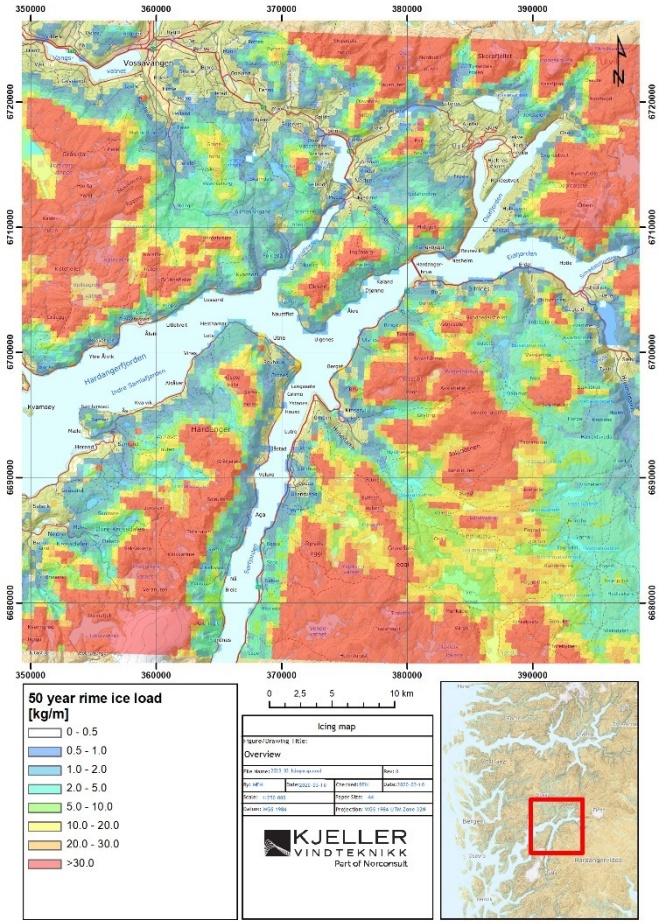

Fig. 8 Preliminary map showing 50-year rime ice loads on a reference object according to [16].

IV. Conclusions and Future Work

Even though the present work is focused on mapping the ice loads in Norway, the methodology and models are general and can be applied in any country or region. However, the importance of local ice load measurements for validation and possibly calibration of the model should be emphasized in any ice load mapping project. The ice load maps based on the assumption of ice accumulation on a reference object can be applied directly as a source of characteristic ice loads for any ground structure covered by the ISO 12494 standard, as well as in future Eurocode parts dealing with actions due to atmospheric icing [22]

While the ice accretion models used to derive these maps includes both melting and sublimation, effects of spontaneous/stochastic ice shedding is not accounted for. For certain types of structures this effect can be significant [2], and the values derived from these maps can therefore be conservative.

The ice load maps for Norway will be completed during the final stage of the Icebox project ending in June 2022. The maps for both rime ice and wet snow with different layers representing the different orientations of the power lines will then be implemented in Statnett's GIS software and made available for the design engineers and route planners. The maps should however be revised and updated in the future along with the continuously increased amount of icing measurements available for validation, as well as with respect to future improvements to the models.

A final remark should be made regarding possible effects of climate change. The maps produced with the presented methodology are based on re-analysis data representing the climate for the last ~30 years. Similar downscaling simulations based on global model simulations of future climate are also possible. Such studies are currently carried out within the Icebox project as presented in [23].

Acknowledgment

The authors would like to thank Statnett and the Norwegian Research Council for funding this work (project NFR 282403).

References

[1] N. D. Mulherin, "Atmospheric icing and communication tower failure in the United States," *Cold Regions Science and Technology,* vol. 27, no. 2, pp. 91-104, 1998.

[2] B. E. Nygaard, H. Ágústsson, L. Moen, Ø. Welgaard and Á. Elíasson, "Monitoring and forecasting ice loads on a 420 kV transmission line in extreme climatic conditions," in *CIGRE*, Paris, 2016.

[3] E. Sundin and N. Mulherin, "Icing-related tower failures in the USA and Fenno–Scandinavia.," in *In Proc. Sixth Int. Workshop on Atmos. Icing of Structures*, 1993.

[4] B. Adum, Ø. Welgaard, A. K. Berstad and M. Radojcic, "Using ice monitoring and modelling to increase reliability and optimise OHTL route planning," in *IWAIS*, Montreal, Canada, 2022.

[5] S. M. Fikke, J. E. Kristjánsson and B. E. Nygaard, "Modern meteorology and atmospheric icing," in *Atmospheric Icing of Power Networks*, Springer, Dordrecht., 2008, pp. 1-29.

[6] B. E. Nygaard, L. Carlshem, J. Bartsch, L. Lee and H. Ágústsson, "Development of a 50-year return value ice load map for Sweden," in *International Workshop on Atmospheric Icing of Structures.*, 2019.

[7] "Icebox project:," Statnett SF, [Online]. Available: https://www.statnett.no/en/about-statnett/innovation-and-technology-development/our-prioritised-projects/icebox/.

[8] W. C. Skamarock, J. B. Klemp, J. Dudhia, D. O. Gill, Z. B. J. Liu and X. Y. Huang, "A description of the advanced research WRF model version 4.," *Atmospheric Research,* 2019.

[9] H. Hersbach, "The ERA5 Atmospheric Reanalysis," in *AGUFM, NG33D-01.*, 2016.

[10] G. Thompson and T. Eidhammer, "A study of aerosol impacts on clouds and precipitation development in a large winter cyclone.," *Journal of the atmospheric sciences,* vol. 71(10, pp. 3636-3658., 2014.

[11] E. C. Iversen, G. Thompson and B. E. Nygaard, "Improvements to melting snow behavior in a bulk microphysics scheme," *J. Atmos. Res.,* vol. 253, p. 105471, 2021.

[12] M. Nakanishi and H. Niino, "Development of an improved turbulence closure model for the atmospheric boundary layer.," *Journal of the Meteorological Society of Japan.,* vol. 87, pp. 895-912., 2009.

[13] M. Iacono, E. Mlawer, S. Clough and J. Morcrette, "Impact of an improved longwave radiation model, RRTM, on the energy budget and thermodynamic properties of the NCAR community climate model, CCM3.," *Journal of Geophysical Research,* 2000.

[14] K. Mitchell, "The Community Noah Land-Surface Model (LSM)," NOAA, Boulder, 2005.

[15] S. Liléo, E. Berge, O. Undheim, R. Klinkert and R. Bredesen, "Long-term correction of wind measurements. State-of-the-art, guidlines and future work.," *Elforsk report,* no. 13:18, 2013.

[16] ISO 12494, "Atmospheric icing of structures, first edition," 2001.

[17] L. Makkonen, "Models for the growth of rime, glaze, icicles and wet snow on structures," *Philosophical Transactions of the Royal Society of London. Series A: Mathematical, Physical and Engineering Sciences,* Vols. 358(1776),, pp. 2913-2939, 2000.

[18] P. Sokolov and M. S. Virk, "Droplet distribution spectrum effects on dry ice growth on cylinders.," *Cold Regions Science and Technology,* vol. 160, pp. 80-88., 2019.

[19] K. Ingvaldsen, B. E. Nygaard, Ø. Byrkjedal and E. C. Iversen, "Validation of Modelled In-cloud Ice Accretion on Overhead Power Lines at Exposed High Altitude Sites in Norway.," in *IWAIS*, 2019.

[20] B. E. Nygaard, H. Ágústsson and K. Somfalvi-Tóth, "Modeling wet snow accretion on power lines: improvements to previous methods using 50 years of observations," *Journal of Applied Meteorology and Climatology,* pp. 2189-2, 2013.

[21] Á. Elíasson, G. Hannesson and E. Thorsteinson, "Wet snow icing—Analysis of field measurements 1999–2016," in *International Workshop on Atmospheric Icing of Structures*, 2017.

[22] B. E. Nygaard, L. Makkonen, B. Wichura, J. Markova and K. Mikulová, "Preparing a European standard for ice loads on structures," in *IWAIS*, Reykjavik, 2019.

[23] E. C. Iversen, B. E. Nygaard, Ø. Hodnebrog, K. Ingvaldsen, M. Sand and Ø. Welgaard, "Future changes of atmospheric icing in Norway," in *IWAIS*, Montreal, 2022.

[24] B. E. Nygaard, Ø. Byrkjedal, E. Iversen, M. Fredbo and H. Ágústsson, "Development of a reliable modelling system for the calculation of rime ice loads on overhead transmission lines," in *IWAIS.*, 2017.

[25] Á. J. Elíasson, H. Ágústsson, G. Hannesson and E. & Thorsteins, "Comparison of measured and simulated icing in 28 test spans during a severe icing episode," in *16th International Workshop on Atmospheric Icing of Structures*, 2015.

[26] B. J. K. Engdahl, B. E. Nygaard, V. Losnedal, G. Thompson and L. Bengtsson, "Effects of the ICE-T microphysics scheme in HARMONIE-AROME on estimated ice loads on transmission lines," *Cold Regions Science and Technology,* vol. 179, p. 103139, 2020.

[27] L. Makkonen, G. Thompson, B. E. Nygaard and P. Lehtonen, "Vertical Distribution of Ice Load on Tall Masts and Towers," *Journal of the International Association for Shell and Spatial Structures (J. IASS),* vol. 55, no. 3, p. 181, 2014.